

## Supplementary Materials for

### Exceptional oxygen evolution reactivities on $\text{CaCoO}_3$ and $\text{SrCoO}_3$

Xiang Li, Hao Wang, Zhiming Cui, Yutao Li\*, Sen Xin, Jianshi Zhou, Youwen Long, Changqing Jin, John B. Goodenough\*

\*Corresponding author. Email: lyththu@utexas.edu (Y.Li.); jgoodenough@mail.utexas.edu (J.B.G.)

Published 9 August 2019, *Sci. Adv.* **5**, eaav6262 (2019)

DOI: 10.1126/sciadv.aav6262

#### This PDF file includes:

Fig. S1. SEM images and particle size distribution of  $\text{CaCoO}_3$  and  $\text{SrCoO}_3$ .

Fig. S2. Elemental distribution of  $\text{CaCoO}_3$  and  $\text{SrCoO}_3$ .

Fig. S3. CV curves of Co-based catalysts.

Fig. S4. Double-layer capacitance measurement to determine the electrochemically active surface area of  $\text{CaCoO}_3$  and  $\text{RuO}_2$ .

Fig. S5. The impedance plots and cycling stability of the catalysts studied in this work.

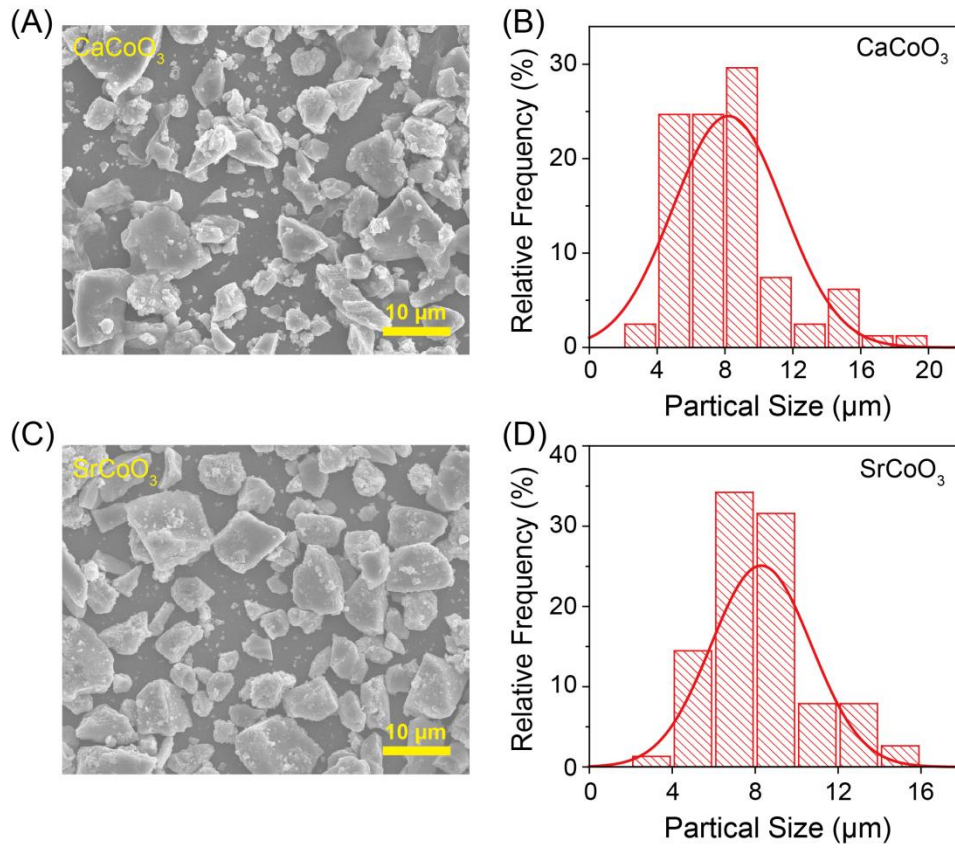
Fig. S6. Response of charge transfer resistance ( $R_{ct}$ ) to applied potential of the catalysts studied in this work to applied potential in the solution of pH 12.5, 13, 13.5, and 14.

Fig. S7. The intermediate spin state of  $\text{Co}^{\text{III}}$  in  $\text{LaCoO}_3$  ( $t^4 e^1$ ,  $S = 1$ ) at  $25^\circ\text{C}$ .

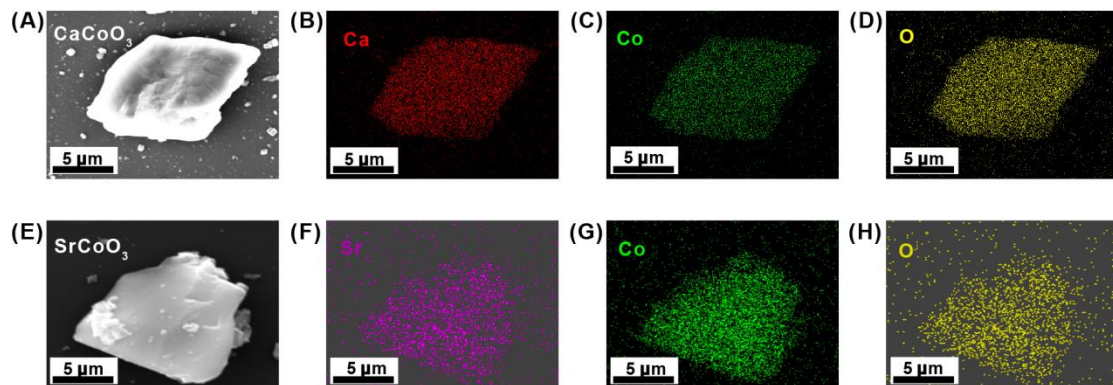
Fig. S8. pH-dependent OER activity of  $\text{RuO}_2$  in  $\text{O}_2$ -saturated KOH with pH 12.5 to 14.

Table S1. Structural refinements of  $\text{CaCoO}_3$  and  $\text{SrCoO}_3$  obtained at room temperature.

Table S2. OER activity and ECSA of all studied catalysts.



**Fig. S1. SEM images and particle size distribution of  $\text{CaCoO}_3$  and  $\text{SrCoO}_3$ .** The particle size distribution was conducted with the software ImageJ.



**Fig. S2. Elemental distribution of  $\text{CaCoO}_3$  and  $\text{SrCoO}_3$ .** EDS mapping of (A to D)  $\text{CaCoO}_3$  and (E to H)  $\text{SrCoO}_3$ .

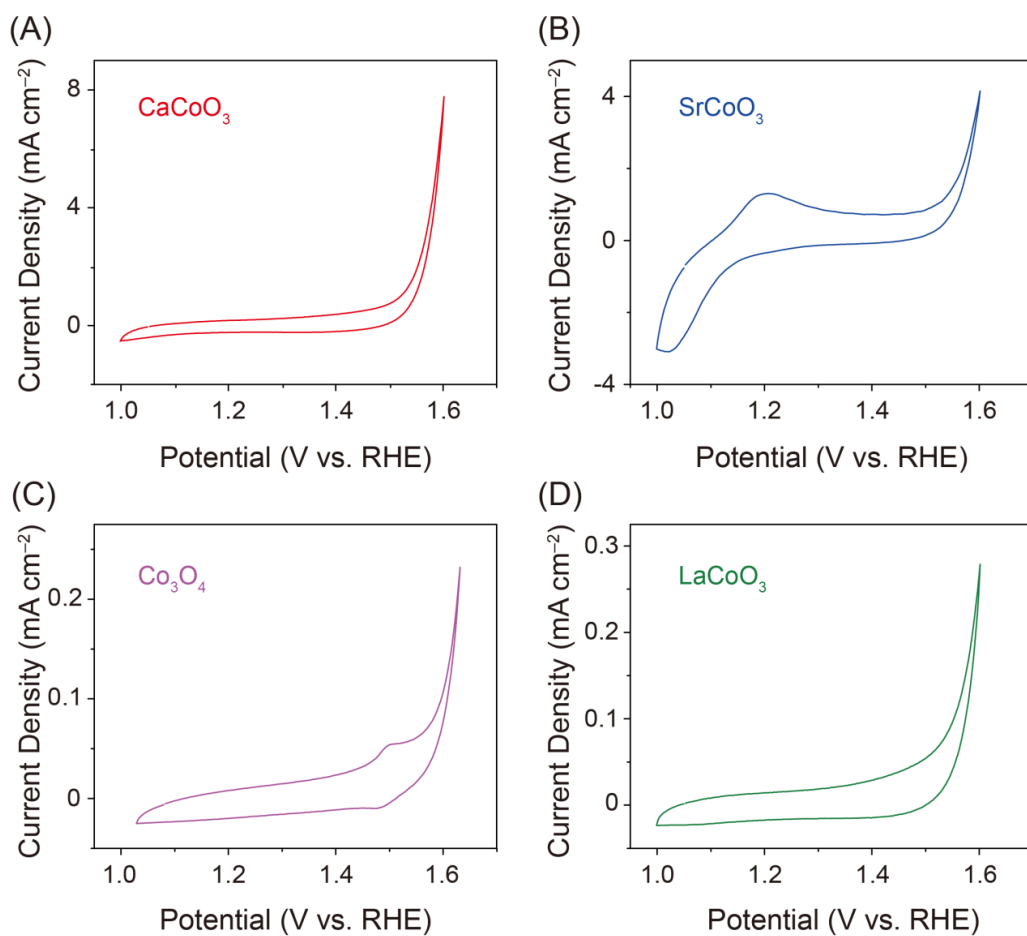


**Fig. S3. CV curves of Co-based catalysts.** (A) CaCoO<sub>3</sub>, (B) SrCoO<sub>3</sub>, (C) Co<sub>3</sub>O<sub>4</sub>, (D) LaCoO<sub>3</sub> at the potential range of 1.0 V to 1.65 V.

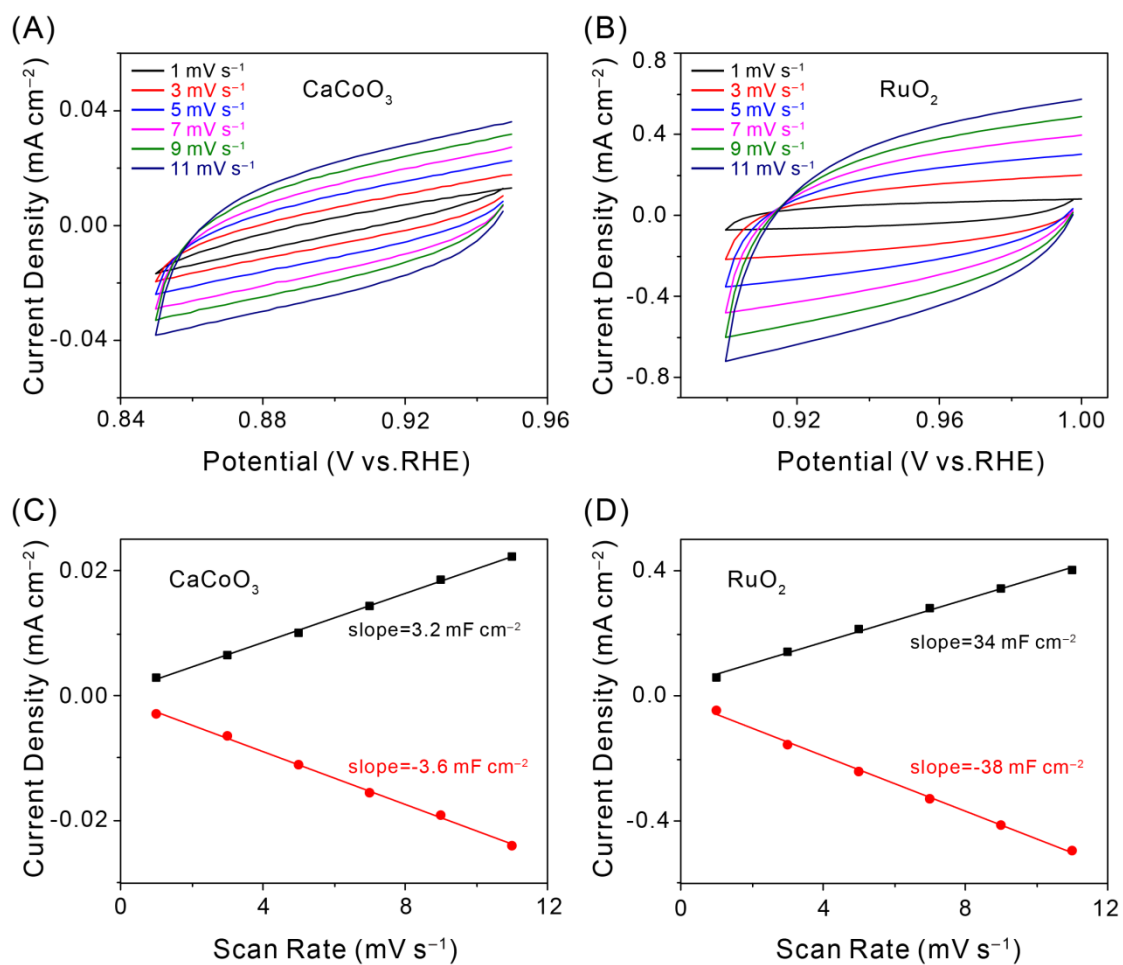


**Fig. S4. Double-layer capacitance measurement to determine the electrochemically active surface area of  $\text{CaCoO}_3$  and  $\text{RuO}_2$ .** CV curves of (A)  $\text{CaCoO}_3$  and (B)  $\text{RuO}_2$  were measured in a non-Faradaic region at scan rates from 1 to 11  $\text{mV s}^{-1}$ ; Current density as a function of the scan rate for (C)  $\text{CaCoO}_3$  at 0.9 V and (D)  $\text{RuO}_2$  at 0.95 V.

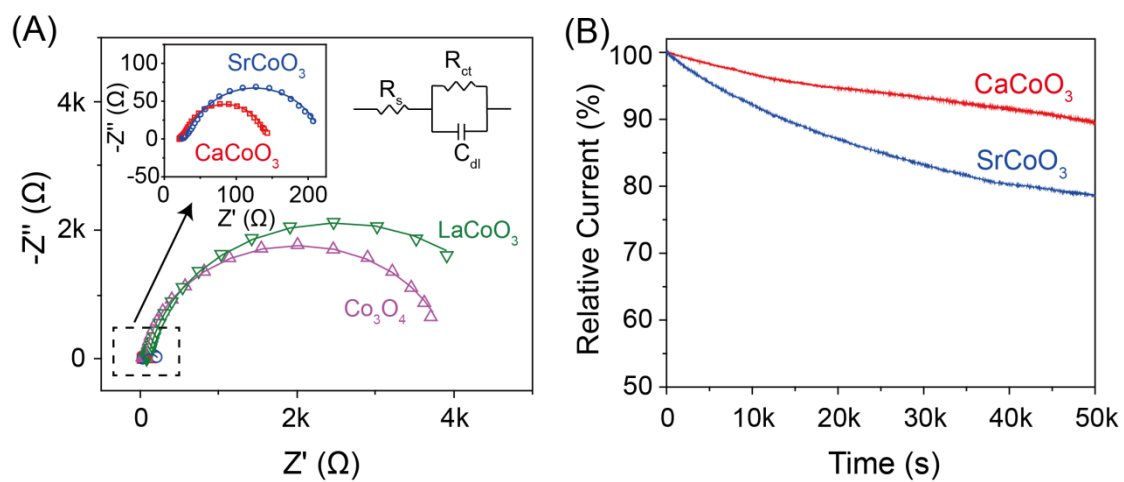


**Fig. S5. The impedance plots and cycling stability of the catalysts studied in this work.**

(A) Nyquist plots and fitting result of the catalysts studied in this work. Inserted is the Electrical equivalent circuit; (B) The chronoamperometric curves of  $\text{CaCoO}_3$  and  $\text{SrCoO}_3$  during 50000 s in an  $\text{O}_2$ -saturated 0.1 M KOH electrolyte at 1.6 V vs. RHE.

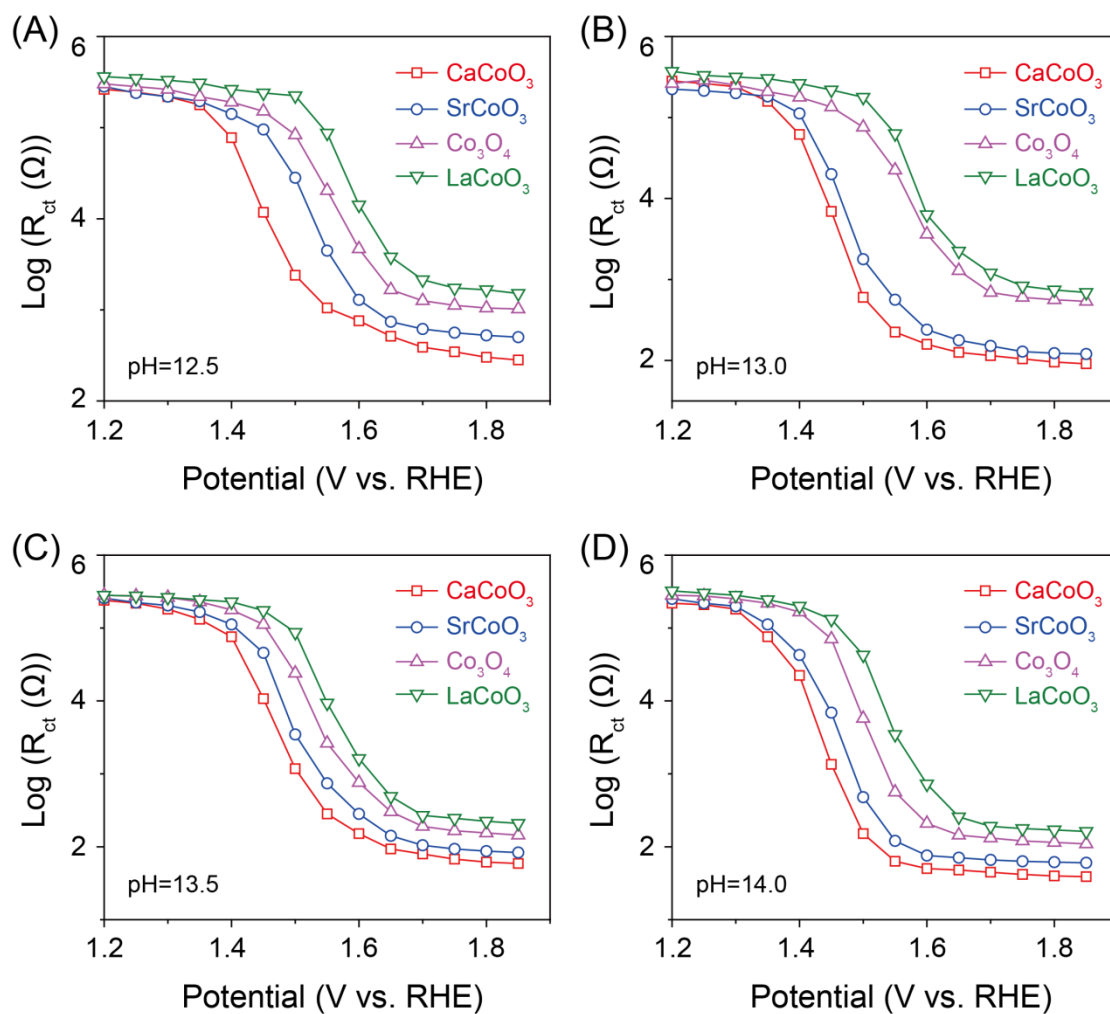


**Fig. S6.** Response of charge transfer resistance ( $R_{ct}$ ) to applied potential of the catalysts studied in this work to applied potential in the solution of pH = 12.5, 13, 13.5 and 14.

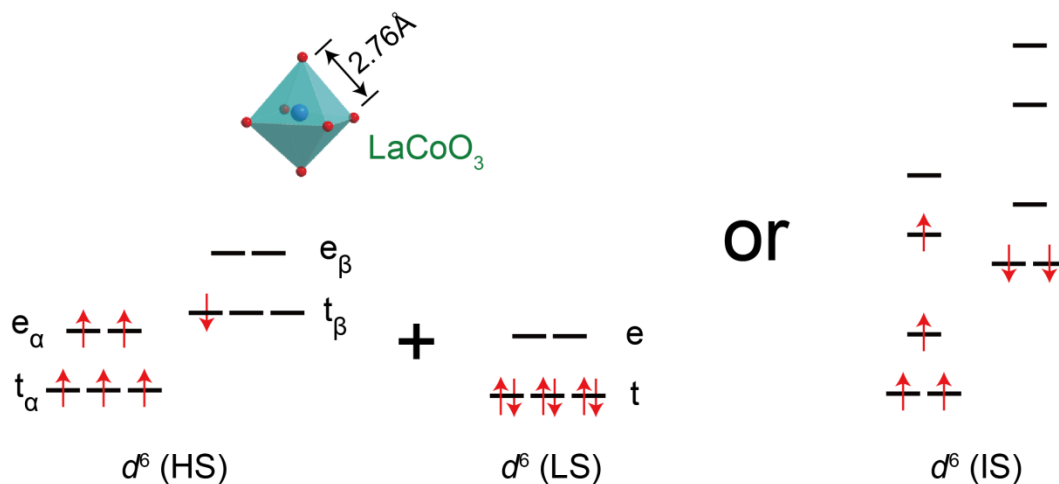


**Fig. S7.** The intermediate spin state (IS) of  $\text{Co}^{\text{III}}$  in  $\text{LaCoO}_3$  ( $t^4e^1$ ,  $S = 1$ ) at 25 °C. There are two possible scenarios to explain the IS mechanism .

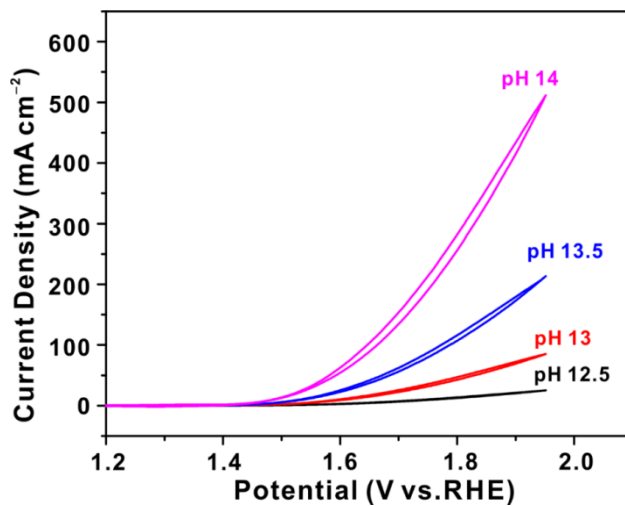


**Fig. S8.** pH-dependent OER activity of  $\text{RuO}_2$  in an  $\text{O}_2$ -saturated KOH with pH 12.5–14.

**Table S1. Structural refinements of CaCoO<sub>3</sub> and SrCoO<sub>3</sub> obtained at room temperature.**

	CaCoO <sub>3</sub>	SrCoO <sub>3</sub>	Co <sub>3</sub> O <sub>4</sub>	LaCoO <sub>3</sub>
<b>Space group</b>	<i>Pm-3m</i>	<i>Pm-3m</i>	<i>Fd-3m</i>	<i>R-3c h</i>
<b>Lattice parameter (Å)</b>	<i>a=b=c=3.734</i>	<i>a=b=c=3.829</i>	<i>a=b=c=0.781</i>	<i>a=b=0.5445, c=1.3093</i>
<b>Atomic positions</b>	Ca (0.5, 0.5, 0.5) Co (0, 0, 0) O (0.5, 0, 0)	Sr (0.5, 0.5, 0.5) Co (0, 0, 0) O (0.5, 0, 0)	Co1 (0, 0, 0) Co2 (0.675, 0.675, 0.675) O (0.388, 0.388, 0.388)	La (0, 0, 0.25) Co (0, 0, 0) O (0.454, 0, 0.25)
<b>Nearest bond length Co-O (Å)</b>	1.867	1.915	1.926	1.930
<b>R<sub>wp</sub> (%)</b>	3.62	3.72		
<b>R<sub>p</sub> (%)</b>	2.84	2.92		
<b>χ<sup>2</sup></b>	1.43	1.53		

Electrochemical double layer capacitance ( $C_{DL}$ ) was determined with cyclic voltammetry measurements. The potential range was determined at a 0.1 V window centered at open-circuit potential (OCP), where there is non-Faradaic current response. CV measurements were conducted in quiescent solution at different scan rates from 1 to 11 mV s<sup>-1</sup>. The  $C_{DL}$  can be calculated by Eq S1

$$j = \nu C_{DL} \quad (S1)$$

$j$  is the current at the central of CV potential range and  $\nu$  is the scan rate. Plotting  $j$  as a function of  $\nu$  yields a straight line with slope equal to  $C_{DL}$ . The electrochemically active surface area (ECSA) of the catalyst can be calculated by dividing  $C_{DL}$  by the specific capacitance ( $C_S$ ) of the sample as shown in Eq S2

$$ECSA = \frac{C_{DL}}{C_S} \quad (S2)$$

Here we use a general specific capacitance ( $C_S$ ) of 0.040 mF cm<sup>-2</sup> for all examples in 0.1 M KOH. The value of  $C_{DL}$  and ECSA of the catalysts were shown in Table S2.

**Table S2. OER activity and ECSA of all studied catalysts.**

<b>Catalyst</b>	<b>Onset potential (V)</b>	<b>Overpotential (V) at 10 mA cm<sup>-2</sup></b>	<b>Tafel slope (mV dec<sup>-1</sup>)</b>	<b>C<sub>DL</sub> (mF)</b>	<b>ECSA (cm<sup>2</sup>)</b>
<b>CaCoO<sub>3</sub></b>	1.48	0.26	42	3.4	85
<b>SrCoO<sub>3</sub></b>	1.51	0.29	49	5.2	130
<b>RuO<sub>2</sub></b>	1.50	0.28	58	36.0	900
<b>Co<sub>3</sub>O<sub>4</sub></b>	1.60	0.43	66	25.2	630
<b>LaCoO<sub>3</sub></b>	1.65	0.49	71	17.8	445